

## Supporting information

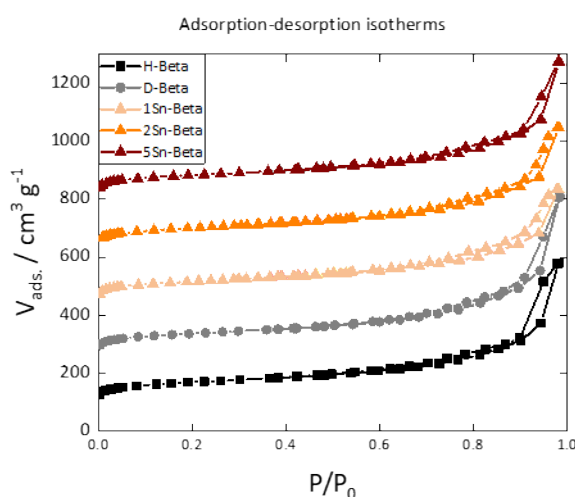
### Lewis acid Sn-Beta catalysts for the cycloaddition of isoprene and methyl acrylate: A greener route to bio-derived monomers

Philipp Treu<sup>[a]</sup>, Philipp Huber<sup>[a]</sup>, Philipp Pleßow<sup>[a]</sup>, Felix Studt<sup>[a,b]</sup>, Erisa Saraci<sup>\*[a,b]</sup>

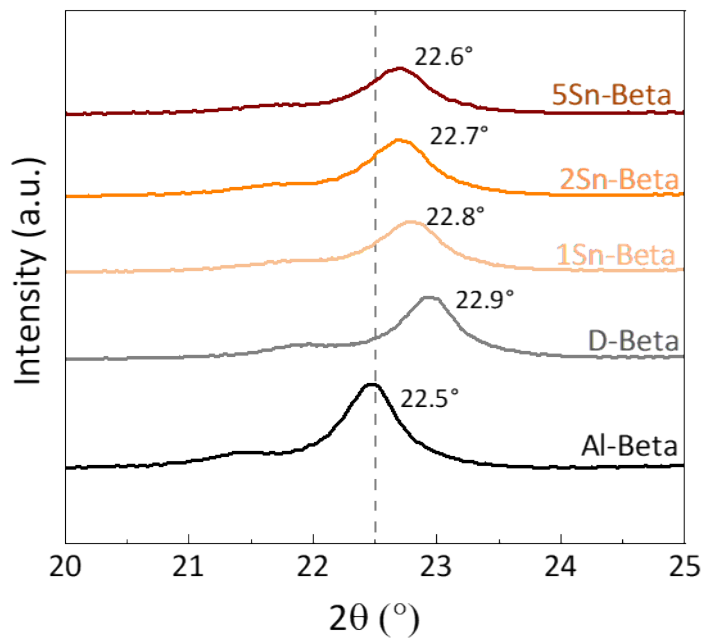
<sup>[a]</sup> Institute of Catalysis Research and Technology, Karlsruhe Institute of Technology (KIT), Hermann-von-Helmholtz-Platz 1, 76344 Eggenstein-Leopoldshafen (Germany)

<sup>[b]</sup> Institute for Chemical Technology and Polymer Chemistry, Karlsruhe Institute of Technology (KIT), Kaiserstraße 12, 76137 Karlsruhe (Germany)

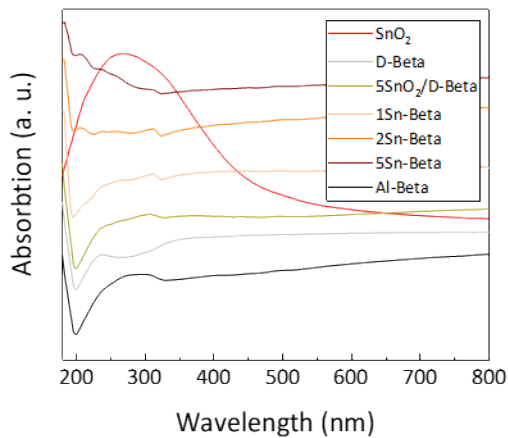
E-mail: erisa.saraci@kit.edu



**Figure S1.** N<sub>2</sub> adsorption-desorption isotherms of parent (Al-Beta), dealuminated (D-Beta) and Sn-substituted Beta zeolites (1, 2, 5Sn-Beta).



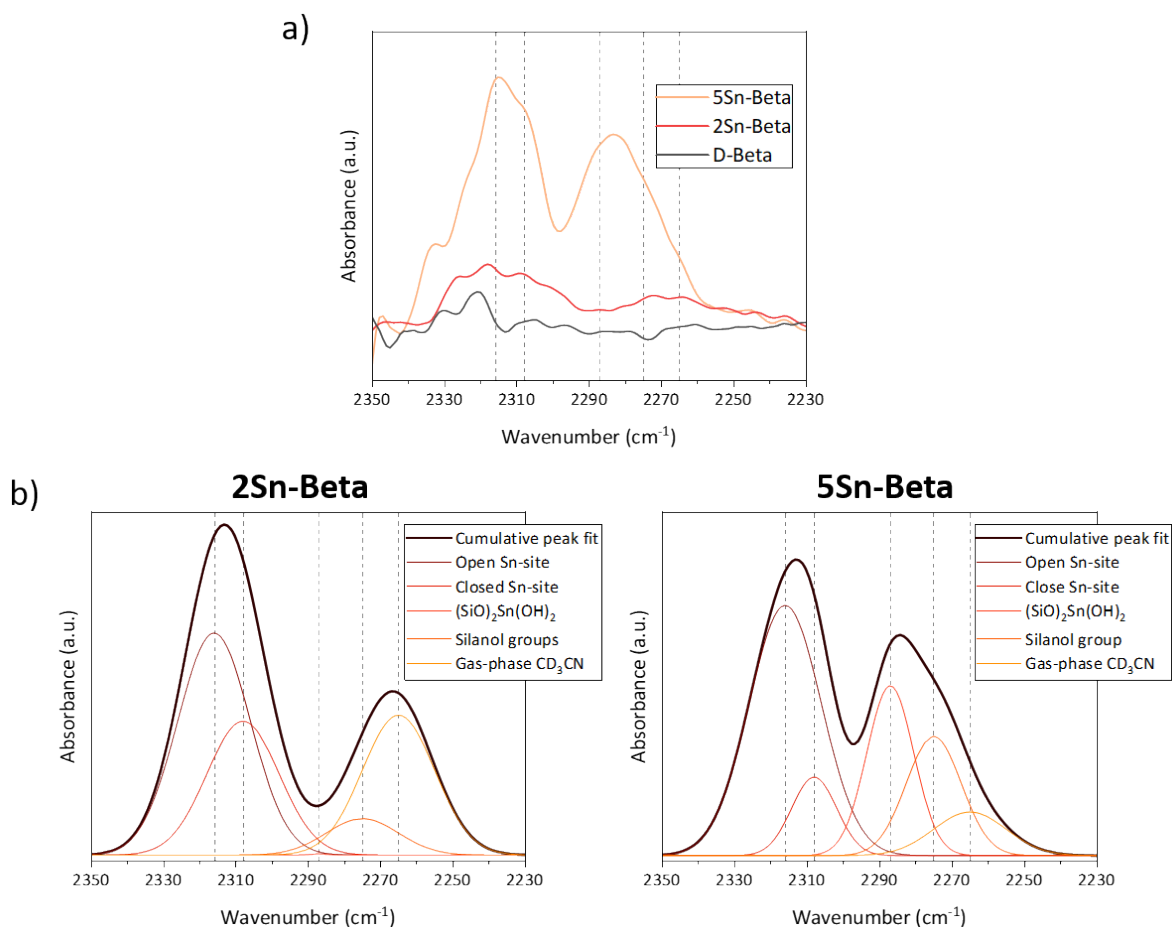
**Figure S2.** XRD diffraction patterns of parent, modified Beta zeolites and  $\text{SnO}_2$  zoomed in the region between 15 and 25 of  $2\theta$  to emphasise the contraction-expansion of the zeolite unit cell volume upon modification of its framework.



**Figure S3.** UV-Vis spectra of parent, dealuminated, and Sn-Beta zeolites as well as reference materials ( $\text{SnO}_2$ , D-Beta and impregnated  $5\text{SnO}_2/\text{D-Beta}$ ).

## Qualitative CD<sub>3</sub>CN-FTIR measurements

A DRIFTS cell (Praying Mantis™, Harrick) equipped with flat CaF<sub>2</sub> windows was loaded with 50 mg of sample in a sieve fraction of 100 – 200 µm. The sample was dehydrated at 673 K in flowing Ar (100 ml/min). Then, the Ar stream was saturated with CD<sub>3</sub>CN at 298 K and passed through the DRIFTS cell for 1 h, saturating the zeolite samples with CD<sub>3</sub>CN. Afterwards, gas-phase CD<sub>3</sub>CN was eliminated by heating the treated sample to 523 K for 30 min in Ar flow (100 ml/min). For the spectra, 128 scans with 4 cm<sup>-1</sup> resolution were taken in the range between 4000 – 800 cm<sup>-1</sup> at 298 K. Spectra of dehydrated samples were used as background for each respective CD<sub>3</sub>CN loaded sample. Deconvolution was performed in Origin applying Gauss fitting to peaks centered at 2316 cm<sup>-1</sup>, 2308 cm<sup>-1</sup>, 2287 cm<sup>-1</sup>, 2275 cm<sup>-1</sup> and 2265 cm<sup>-1</sup>, restraining full width half maximums between 5 to 20 cm<sup>-1</sup>.



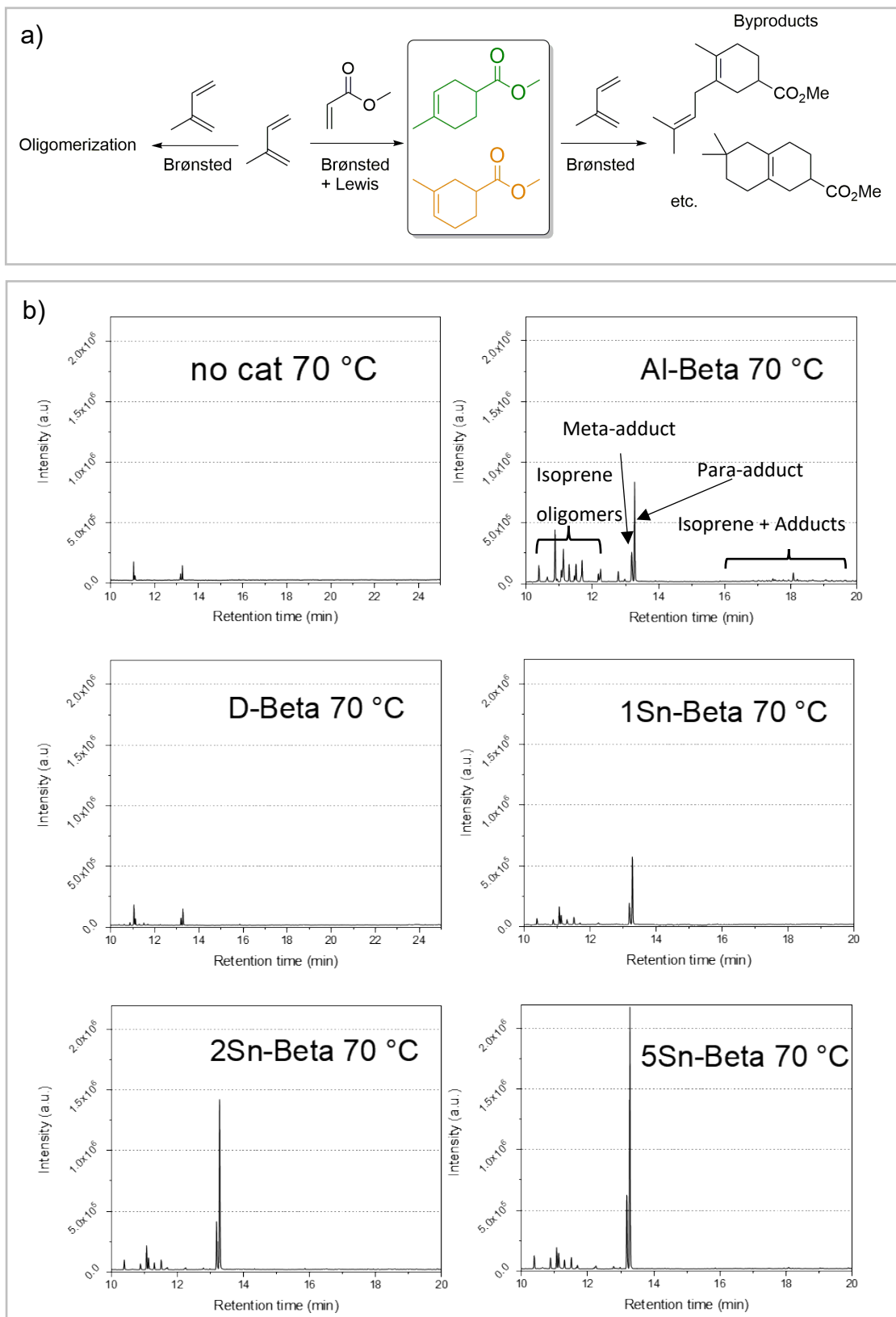
**Figure S4.** DRIFT spectra of CD<sub>3</sub>CN adsorbed samples. Reference lines refer to open Sn-sites (2316 cm<sup>-1</sup>), closed Sn-sites (2308 cm<sup>-1</sup>), (SiO)<sub>2</sub>Sn(OH)<sub>2</sub>-sites (2287 cm<sup>-1</sup>), silanol groups (2275 cm<sup>-1</sup>), and gas-phase CD<sub>3</sub>CN (2265 cm<sup>-1</sup>).<sup>1</sup> a) Comparison of spectra for D-Beta, 2Sn-Beta and 5Sn-Beta. b) Peak deconvolution of spectra for 2Sn-Beta (left) and 5Sn-Beta (right), including cumulative peak fit.

Figure S4 a) shows the adsorbed CD<sub>3</sub>CN DRIFT spectra on D-Beta, 2Sn-Beta and 5Sn-Beta. D-Beta does not show any significant absorption bands. For the Sn-Beta zeolites, 5Sn-Beta shows stronger absorption bands compared to 2Sn-Beta, probably due to higher density of Sn-sites. Both 2Sn-Beta and 5Sn-Beta show two absorption bands,

one from  $2330\text{ cm}^{-1}$  to  $2300\text{ cm}^{-1}$  and the other from  $2300\text{ cm}^{-1}$  to  $2260\text{ cm}^{-1}$ . Deconvoluting the first band into component peaks indicate the presence of open ( $2316\text{ cm}^{-1}$ ) and closed ( $2308\text{ cm}^{-1}$ ) Sn-sites.<sup>1</sup> Integrals of absorption bands for open and closed Sn-sites for 2Sn-Beta and 5Sn-Beta suggest that with higher loading, more open Sn-sites are formed. However, while the reaction rate increases with Sn-loading, the catalytic activity per Sn site (TON) is lower for 5Sn-Beta relative to 2Sn-Beta. Therefore, although these results give us the impression that closed Sn-sites are of higher importance for this catalysis, a clear correlation between the nature of the Sn-sites with the activity cannot be drawn. The deconvolution of the second absorption bands from  $2300\text{ cm}^{-1}$  to  $2260\text{ cm}^{-1}$  reveal the presence of  $(\text{SiO})_2\text{Sn(OH)}_2$ -sites ( $2287\text{ cm}^{-1}$ ), silanol groups ( $2275\text{ cm}^{-1}$ ), and residual gas-phase  $\text{CD}_3\text{CN}$  ( $2265\text{ c}^{-1}$ ).<sup>1</sup> The resulting peak for silanol groups at  $2275\text{ cm}^{-1}$  is similar for both 2Sn- and 5Sn-Beta, which is to be expected since both catalysts are prepared from the same starting material and same batch of dealuminated Beta zeolite (D-Beta). Further, peak deconvolution suggests that  $(\text{SiO})_2\text{Sn(OH)}_2$ -sites are significantly dominant in 5Sn-Beta as compared to 2Sn-Beta. A possible explanation for this might be the higher deposition of Sn on the external surface of the zeolite, leading to the formation of highly defective  $(\text{SiO})_2\text{Sn(OH)}_2$ -sites.<sup>1</sup>

#### Reference

- 1 J. W. Harris, M. J. Cordon, J. R. Di Iorio, J. C. Vega-Vila, F. H. Ribeiro and R. Gounder, *Journal of Catalysis*, 2016, 335, 141–154.



**Figure S5.** a) Reaction scheme of main reaction and possible side reactions and b) GC-MS analysis of the product solutions obtained from the reaction using all catalyst at 70 °C, 5 h,  $n_{\text{isoprene}}:n_{\text{methyl acrylate}} = 3$ , 100 mg 70 °C. Significant peaks for desired products and by-products are shown in the GC-MS chromatogram for Al-Beta.

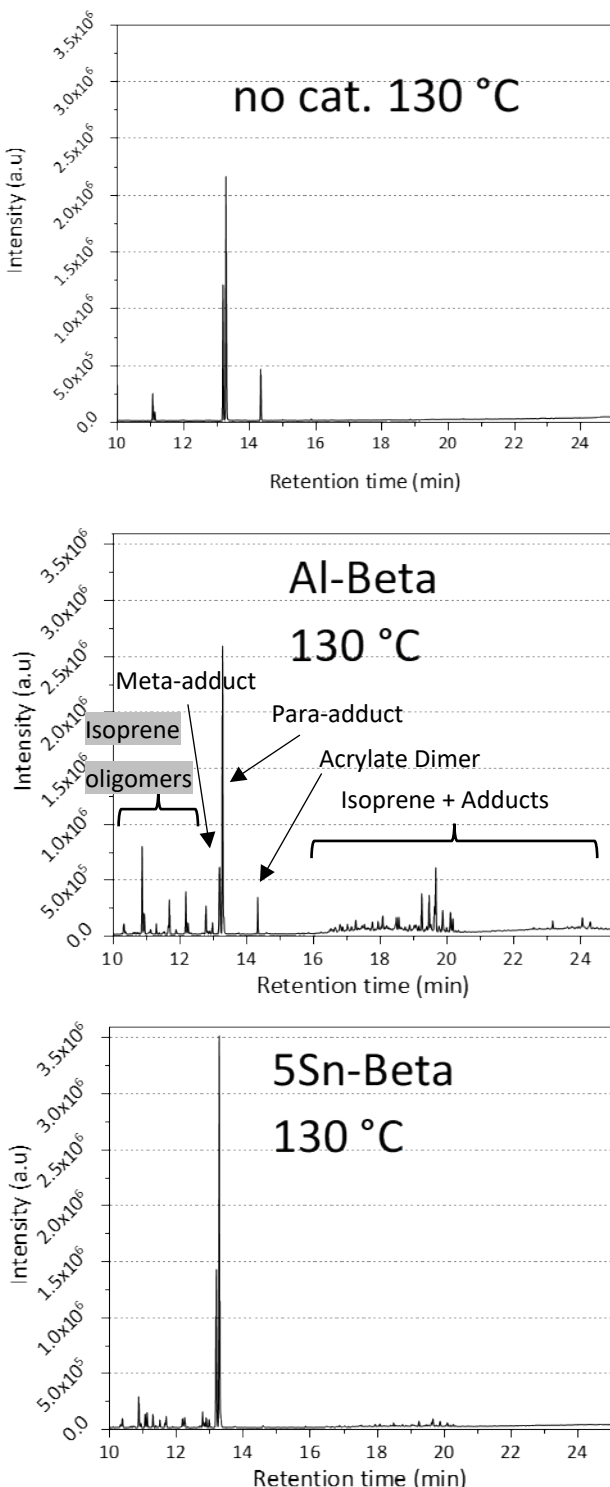


**Figure S6.** GC-MS analysis of the product solution obtained from the reaction using no catalyst, Al-Beta and 5Sn-Beta respectively at 130 °C, 5 h,  $n_{\text{isoprene}}:n_{\text{methyl acrylate}} = 3$ , 100 mg 70 °C. Significant peaks for desired products and by-products are shown in the GC-MS chromatogram for Al-Beta.

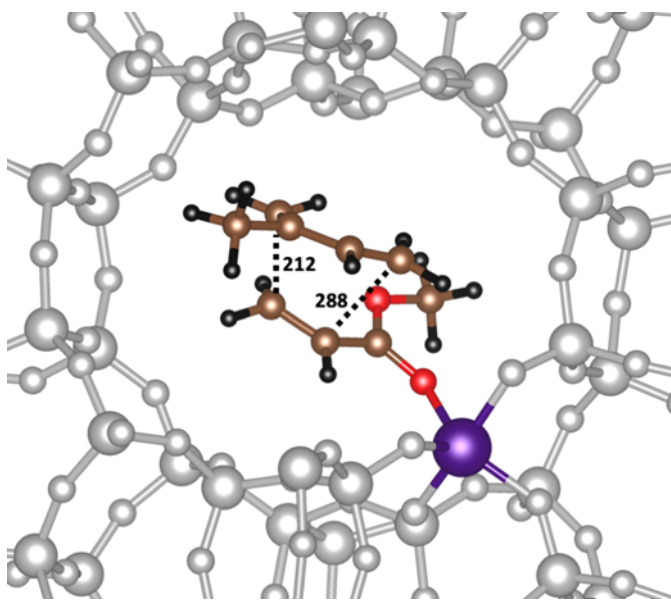


**Figure S7.** Computed DA transition state ((R) – para-/exo) structure on the Sn-Beta T8 site. Depicted distances are in picometers. Strong adsorption of methyl acrylate  $\approx$  1 eV. Adsorption of 2nd methyl acrylate  $\approx$  0.7 eV. Additional isoprene adsorption also  $\approx$  0.7 eV.

**Table S1.** Calculated energy barriers for transition states at Sn-Beta T8 site in right handed Beta polymorph A. Lowest energy barriers for each pair of enantiomers are shown in bold.

Transition state coordination	Energy barrier (kJ/mol)
(R) - meta/endo	30
(S) - meta/endo	<b>26</b>
(R) - meta/exo	<b>20</b>
(S) - meta/exo	32
(R) - para/endo	<b>41</b>
(S) - para/endo	57
(R) - para/exo	<b>13</b>
(S) - para/exo	28

**Table S2.** Calculated energy barriers for transition states at Al-Beta T8 site in right handed Beta polymorph A. All four surrounding O-atoms of Al at the T8 site and only transition states leading to the (S)-enantiomer have been considered.

Transition state coordination	o1	o2	o3	o4
(S) - meta/endo	43	<b>35</b>	58	36
(S) - meta/exo	<b>16</b>	38	41	40
(S) - para/endo	50	<b>33</b>	59	34
(S) - para/exo	<b>11</b>	13	32	31

Calculations show a slight preference towards the *para*-adduct on the Al-Beta T8 site in right handed Beta polymorph A, by 5 kJ/mol. Calculation results are in agreement with experimental results, where the use of Al-Beta led to a *para/meta*-ratio of 5.4. Barriers for the *exo* transition states are similar (maximum difference of 4 kJ/mol). When comparing transition states in Al-Beta and Sn-Beta. Differences for *endo* transition states are slightly larger (maximum difference of 8 kJ/mol).

**Table S3.** Periodic PBE-D3 energies and corresponding D3 contribution in eV.

System	PBE-D3	D3
H2O_g	-14.225	-0.000
pyridine_g	-71.320	-0.073
isoprene_g	-73.769	-0.102
MA_g	-71.135	-0.096
Al-Beta	-1533.307	-11.579
Sn_Beta	-1525.300	-11.594
Al-Beta_Py_O1	-1606.633	-12.224
Al-Beta_Py_O2	-1606.740	-12.211
Al-Beta_Py_O3	-1606.626	-12.359
Al-Beta_Py_O4	-1606.459	-12.297
Sn-Beta_H2O	-1540.272	-11.766
Sn-Beta_H2O_Py	-1613.063	-12.430
Sn-Beta_Py	-1598.062	-12.318
Sn_precursor	-1671.822	-13.257
Sn_ts_meta_endo_R	-1671.508	-13.420
Sn_ts_meta_endo_S	-1671.550	-13.394
Sn_ts_meta_exo_R	-1671.614	-13.241
Sn_ts_meta_exo_S	-1671.490	-13.353
Sn_ts_para_endo_R	-1671.394	-13.465
Sn_ts_para_endo_S	-1671.228	-13.465
Sn_ts_para_exo_R	-1671.688	-13.266
Sn_ts_para_exo_S	-1671.529	-13.268
Al_precursor	-1680.154	-13.199
Al_ts_meta_endo_S_O1	-1679.707	-13.308
Al_ts_meta_endo_S_O2	-1679.791	-13.379
Al_ts_meta_endo_S_O3	-1679.556	-13.431
Al_ts_meta_endo_S_O4	-1679.786	-13.299
Al_ts_meta_exo_R_O1	-1679.934	-13.059
Al_ts_meta_exo_R_O2	-1679.910	-13.174
Al_ts_meta_exo_R_O3	-1679.902	-13.228
Al_ts_meta_exo_R_O4	-1679.901	-13.218
Al_ts_meta_exo_S_O1	-1679.989	-13.142
Al_ts_meta_exo_S_O2	-1679.761	-13.142
Al_ts_meta_exo_S_O3	-1679.733	-13.133

Al_ts_meta_exo_S_O4	-1679.741	-13.147
Al_ts_para_endo_S_O1	-1679.636	-13.375
Al_ts_para_endo_S_O2	-1679.809	-13.280
Al_ts_para_endo_S_O3	-1679.539	-13.279
Al_ts_para_endo_S_O4	-1679.800	-13.271
Al_ts_para_exo_S_O1	-1680.037	-13.157
Al_ts_para_exo_S_O2	-1680.019	-13.146
Al_ts_para_exo_S_O3	-1679.827	-13.146
Al_ts_para_exo_S_O4	-1679.831	-13.150
gas_precursor	-144.957	-0.375
gas_ts_meta_endo_S	-144.519	-0.410
gas_ts_meta_exo_S	-144.483	-0.375
gas_ts_para_endo_S	-144.528	-0.399
gas_ts_para_exo_S	-144.515	-0.375

**Table S4.** Harmonic frequencies in cm<sup>-1</sup>.

System	Frequencies
H2O_g	1579.0, 3697.3, 3812.2
pyridine_g	20.3i, 14.3i, 4.6i, 22.5, 39.1, 43.9, 357.5, 399.1, 593.1, 646.6, 692.4, 740.4, 868.2, 922.2, 965.4, 981.1, 982.8, 1024.2, 1051.6, 1067.2, 1139.6, 1209.4, 1299.0, 1336.2, 1427.0, 1463.1, 1575.5, 1578.1, 3066.3, 3068.7, 3094.4, 3109.4, 3118.2
Al-Beta	195.5, 213.1, 215.9, 228.4, 270.2, 275.1, 306.1, 329.1, 355.2, 361.2, 385.9, 487.7, 497.9, 592.3, 623.0, 637.9, 645.5, 651.3, 659.8, 666.9, 682.1, 705.3, 734.6, 750.6, 781.9, 1089.3, 1105.5, 1128.1, 1147.9, 3484.7
Sn_Beta	122.0, 139.1, 140.9, 205.1, 226.2, 241.0, 252.2, 326.6, 337.9, 361.5, 364.9, 542.3, 562.9, 585.4, 589.8, 642.5, 647.9, 651.0, 655.0, 671.7, 677.2, 682.8, 689.0, 949.3, 956.9, 957.8, 1040.3
Al-Beta_Py_O1	29.9, 48.5, 62.0, 88.9, 104.6, 111.1, 197.0, 218.1, 223.4, 254.8, 283.8, 293.8, 342.1, 342.7, 348.5, 390.6, 393.4, 402.7, 428.8, 558.4, 598.5, 614.5, 621.6, 629.8, 633.8, 637.4, 640.1, 649.3, 660.2, 663.0, 673.2, 685.5, 692.2, 721.1, 747.5, 863.7, 933.8, 978.0, 989.5, 1002.9, 1009.3, 1021.0, 1062.5, 1065.9, 1072.5, 1095.1, 1133.6, 1152.8, 1162.4, 1194.4, 1298.8, 1345.9, 1399.7, 1475.5, 1548.8, 1625.7, 1635.0, 2614.4, 3113.2, 3135.6, 3138.4, 3147.1, 3155.6
Al-Beta_Py_O2	50.7, 65.6, 71.4, 80.7, 114.5, 117.4, 191.1, 214.1, 229.3, 250.9, 284.3, 287.2, 337.1, 344.4, 346.6, 393.4, 398.5, 400.4, 415.6, 558.0, 601.2, 612.6, 620.9, 632.0, 633.3, 636.3, 639.0, 648.4, 658.3, 664.0, 669.6, 689.4, 697.4, 716.4, 759.8, 877.9, 940.3, 989.8, 999.8, 1010.9, 1024.7, 1025.5, 1059.6, 1063.3, 1064.9, 1086.4, 1098.9, 1142.9, 1163.5, 1193.7, 1289.3, 1345.8, 1393.8, 1475.0, 1543.0, 1622.5, 1626.4, 2867.7, 3115.4, 3142.2, 3146.3, 3155.2, 3158.2
Al-Beta_Py_O3	25.7, 61.3, 67.7, 75.3, 105.4, 113.9, 213.9, 217.3, 232.2, 243.5, 270.1, 295.1, 319.8, 348.9, 369.7, 373.4, 395.4, 399.7, 409.7, 552.4, 600.1, 617.2, 620.5, 625.4, 630.5, 635.7, 642.7, 644.8, 653.7, 662.8, 667.0, 684.7, 716.6, 718.8, 745.4, 863.5, 938.6, 977.1, 992.9, 1007.5, 1010.8, 1022.9, 1062.2, 1062.9, 1084.5, 1112.4, 1142.6, 1156.0, 1164.5, 1194.7, 1294.8, 1346.9, 1389.0, 1476.1, 1541.1, 1617.8, 1629.1, 2720.5, 3123.2, 3132.9, 3138.4, 3149.9, 3153.7
Al-Beta_Py_O4	29.1, 45.5, 62.0, 76.4, 86.1, 108.0, 203.5, 210.5, 229.6, 247.7, 275.0, 289.0, 327.0, 344.2, 358.5, 380.7, 390.8, 394.2, 405.4, 552.5, 598.7, 619.0, 624.4, 632.4, 633.6, 635.8, 644.5, 647.4, 651.8, 666.3, 673.2, 676.7, 707.7, 733.2, 747.1, 866.9, 924.8, 979.0, 996.5, 1010.5, 1015.4, 1021.6, 1042.7, 1058.6, 1064.0, 1068.9, 1111.3, 1158.3, 1158.9, 1198.4, 1298.2, 1345.2, 1395.2, 1474.2, 1547.5, 1626.0, 1631.3, 2924.9, 3114.1, 3117.7, 3135.9, 3138.0, 3159.4
Sn-Beta_H2O	113.1, 122.1, 152.3, 157.7, 172.3, 221.9, 254.2, 257.1, 262.0, 287.0, 348.7, 351.7, 364.5, 374.5, 382.3, 542.8, 551.6, 564.8, 583.2, 601.8, 625.2, 632.6, 645.9, 651.3, 665.6, 672.9, 674.4, 682.3, 772.1, 958.6, 977.2, 982.1, 1047.8, 1548.3, 3408.1, 3702.8
Sn-Beta_H2O_Py	38.2, 49.1, 69.8, 77.8, 85.5, 106.2, 118.8, 130.0, 159.3, 177.0, 209.6, 251.2, 256.4, 286.6, 309.7, 346.8, 364.2, 367.3, 374.5, 391.3, 405.0, 444.9, 499.8, 532.7, 537.8, 570.3, 570.9, 597.9, 618.4, 635.6, 638.2, 639.3, 643.2, 647.9, 654.0, 659.5, 667.2, 688.1, 746.9, 863.5, 885.6, 939.8, 971.9, 974.4, 985.7, 997.4, 1008.3, 1010.0, 1023.3, 1062.1, 1065.5, 1068.0, 1156.6, 1195.7, 1236.4, 1310.5, 1344.1, 1412.3, 1477.1, 1556.9, 1622.0, 1659.0, 2113.3, 3114.5, 3130.7, 3142.6, 3143.0, 3153.9, 3686.4
Sn-Beta_Py	15.9, 40.5, 60.1, 99.3, 119.1, 129.9, 164.3, 170.2, 197.7, 225.7, 252.4, 258.3, 283.0, 311.2, 348.9, 358.9, 370.1, 385.3, 422.5, 528.0, 538.6, 580.4, 585.7, 621.3, 628.3, 637.1, 640.5, 644.0, 647.8, 653.0, 664.6, 666.9, 675.7, 690.9, 750.9, 864.1, 946.2, 971.7, 976.8, 995.1, 1000.4, 1001.1, 1006.8, 1028.9, 1060.3, 1070.7, 1077.4, 1151.2, 1210.3, 1305.0, 1339.4, 1436.4, 1470.4, 1570.1, 1601.5, 3104.7, 3125.2, 3128.5, 3150.8, 3162.5

**Table S5.** Computed and experimental 19b frequencies (shift to gas phase) in cm<sup>-1</sup>.

System	19b Frequency (cm <sup>-1</sup> )	
	computed	experimental
gas phase	1427	1440
Al-Beta*pyridine	1543 (Δv = 116)	1549 (Δv = 109)
Sn-Beta*pyridine	1436 (Δv = - 9)	1436 (Δv = - 4 )
Sn-Beta*H <sub>2</sub> O*pyridine	1557 (Δv = 130)	1549 (Δv = 109)